Resonant Reflection From Cylindrical Grating-Waveguide Under Holistic Excitation

Erieta Katerina Koussi, Hugo Bruhier, Maria Alejandra Usuga Higuita, Isabelle Verrier, Colette Veillas, Thomas Kampfe, Stéphanie Reynaud, Nicolas Crespo-Monteiro, Olivier Parriaux, Yves Jourlin

IEEE Photonics Journal
An IEEE Photonics Society Publication

Open Access

Resonant Reflection From Cylindrical Grating-Waveguide Under Holistic Excitation

Volume 12, Number 2, April 2020

Erieta Katerina Koussi
Hugo Bruhier
M. A. Usuga Higuita
Isabelle Verrier
Colette Veillas
Thomas Kämpfe
Stephanie Reynaud
Nicolas Crespo-Monteiro
Olivier Parriaux
Yves Jourlin

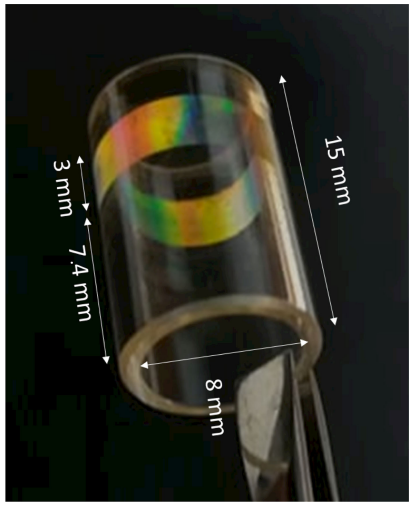

DOI: 10.1109/JPHOT.2020.2966146

Resonant Reflection From Cylindrical Grating-Waveguide Under Holistic Excitation

Erieta Katerina Koussi, Hugo Bruhier, M. A. Usuga Higuita, Isabelle Verrier, Colette Veillas, Thomas Kämpfe, Stephanie Reynaud, Nicolas Crespo-Monteiro, Olivier Parriaux, and Yves Jourlin

Université de Lyon, UJM-Saint-Etienne, CNRS, Institut d'Optique Graduate School, Laboratoire Hubert Curien, UMR CNRS 5516, 42000 Saint-Etienne, France

DOI:10.1109/JPHOT.2020.2966146

Manuscript received October 24, 2019; revised January 8, 2020; accepted January 9, 2020. Date of publication January 12, 2020; date of current version March 9, 2020. This work was supported by LABEX MANUTECH-SISE (ANR-10-LABX-0075) of Université de Lyon, within the program "Investissements d'Avenir" (ANR-11-IDEX-0007) operated by the French National Research Agency (ANR). Corresponding author: Isabelle Verrier (e-mail: isabelle.verrier@univ-st-etienne.fr).

Abstract: The phenomenon of resonant reflection from a grating-coupled waveguide mode is conceptually, technologically, and experimentally transposed from a planar corrugated waveguide structure under plane wave excitation to a circularly symmetrical waveguide at the inner wall of a tube under cylindrical wave excitation. The mode coupling element is an azimuthally periodic wall corrugation having an integer number of lines parallel to the tube axis. The grating is defined by diffractive coordinate transform of a radial grating phase-mask transverse to the tube axis under axial beam exposure onto a photoresist-coated TiO_2 sol-gel wall-waveguide. The holistic excitation of a waveguide mode is achieved by transforming a broad spectrum, centered axial incident beam into a cylindrical wave by a centered, 90° apex reflective cone. The expected resonantly reflected cylindrical wave at the mode-coupling wavelength is in turn transformed back into an axial beam by the cone. TE resonant reflection is demonstrated experimentally.

Index Terms: Cylindrical resonant grating.

1. Introduction

The present work reports on the attempt to transpose the known [1] and since then widely analyzed [2], and applied [3] resonant effect of anomalous reflection from a planar corrugated slab waveguide into the 3D space of a cylindrical geometry. This effect, now called GMR Guided-Mode Resonance, manifests itself as a narrow polarization, wavelength and angularly dependent theoretically 100% reflection peak as the phase-matching condition for the excitation of a waveguide mode is satisfied. The transposition to a cylindrical geometry is all at once a conceptual, technological and experimental problem. Besides, novel diffractive functions, devices, and applications naturally emerge after a specific spatial coherence quantification condition has been satisfied: the number of the coupling grating lines at the wall of a circularly symmetrical cylindrical waveguide of radius R at which a cylindrical wave impinges must be an integer number N. This leads to the definition of an angular period $\Lambda_\phi = 2\pi/N$ in radians and to the related period Λin length units at the periphery of

the cylinder wall $\Lambda = 2\pi R/N = R\Lambda_\phi$. Generating a cylindrical wave from a collimated axial beam is easy: a reflective cone of 90° apex angle and axis parallel to the k-vector of the incident beam gives rise to a cylindrical wave whose k-vector is in a plane orthogonal to the incident beam axis. A TE (TM) cylindrical wave incident on the cylindrical wall grating corresponds to a radially (azimuthally) polarized state of the incident axial beam on the reflective cone. Most difficult is however the fabrication of a cylindrical grating having an integer number of wavelength-scale submicron periods at the wall of a cylinder; usual methods for plane gratings such as interferogram projection, optical or mechanical ruling are by far inappropriate. A perceptive fabrication strategy was found [4] that uses high-end surface patterning technologies of microelectronics, e.g., electron beam writing, for the very accurate definition of a master pattern, and to define an optical projection scheme capable of transforming the planar pattern into a set of *N* straight lines in a 3D cylindrical coordinate system. This is exactly what a planar phase-mask composed of an integer number of radial lines does when illuminated by an axial beam under normal incidence: The local transmitted $+$ and -1st diffraction orders have axial, radial and azimuthal components; they interfere everywhere including at the wall of a cylinder whose axis contains the phase-mask center in the form of a set of lines parallel to the axis, the number *N* of lines being exactly twice the integer number of periods of the radial grating phase-mask. The interference contrast at the cylinder wall is large since the 0th transmitted order, which is difficult to extinguish, propagates parallel to the axis, thus does not overlap with the two orders interfering at the wall [5].

The cylindrical analogue of a planar dual-grating translation sensor [6] was conceived to serve as a high-resolution rotation sensor encompassing two cylindrical gratings, one transmissive of angular period Λ_ϕ, an outer reflective grating of period $\Lambda_\phi/2$, and a reflective cone to convert an axial incident beam into a cylindrical wave and conversely. The power of the returned beam is modulated at the rate of the rotation of one of the gratings relative to the other.

The new structure and related optical function reported here involves a cylindrical grating waveguide defined at the inner wall of a transparent glass tube. It comprises a uniform TiO_2 sol-gel layer that acts as an optical waveguide, and a grating defined in a photoresist overlay by phase-mask projection as described above. In a cylindrical geometry the waveguide-mode coupling and expected resonant reflection occur identically over 2π if the waveguide layer and resist thickness is azimuthally uniform. As the incidence is locally normal, the mode coupling condition is $n_e(\lambda)k_0 = K_g$ where $k_0 = 2\pi/\lambda$is the wave vector modulus in vacuum, $n_e(\lambda)$ the effective index of the coupled mode of the layer/photoresist assembly at wavelength λ, and $K_g = 2\pi/\Lambda$ is the grating constant. Assuming the coupling condition to be satisfied at wavelength λ, the phase $\Delta\Phi$ of the coupled mode accumulated over a round-trip $L = 2\pi R = N\Lambda$ is $\Delta\Phi = n_e(\lambda)k_0L = K_gL = 2\pi N$, thus the number of periods being an integer *N* ensures that the phase accumulated by the coupled waveguide mode over *L* is an integer number of 2π. This implies that the grating-coupled wall-waveguide can be considered as a multi-turn ring resonator provided the scattering and absorption losses of the coupled mode are small enough, and the propagation length L_p of the coupled mode, given as the inverse of the radiation coefficient of the grating waveguide [7] larger or much larger than *L*.

The technical content of the present paper encompasses the design of the structure, its fabrication technology, and the experimental demonstration of the resonant reflection of a cylindrical wave at the inner-wall grating waveguide. Section 2 concerns the structure dimensioning for near-IR operation considering a uniform sol-gel waveguide and a photoresist grating. The theoretical modeling is carried out in a planar geometry; this is legitimate since the inner-wall curvature radius is as large as 4 mm, and the waveguide and grating refractive index is in the range of 1.7 against 1.45 for the fused silica tube material. The outcome of Section 2 is the grating period, the waveguide and grating thicknesses, and the expected spectral position of the TE_0 and TM_0 waveguide mode reflection peaks. Section 3 describes the waveguide and grating technologies, and puts the emphasis on the phase-mask transfer principle, and on the critical exposure conditions leading to a well-defined, high-efficiency grating waveguide at the silica tube inner wall. Section 4 reports on the design of the cylindrical grating waveguide functional characterization using a reflective cone to transform the axial incident beam into the cylindrical wave impinging on the corrugated wall waveguide, and finally

Section 5 shows the experimental reflection spectrum, compares it with the theoretical model, and concludes.

In a previous paper [4] we demonstrated the fabricability of a cylindrical grating at the outer wall of a fused quartz solid cylinder having an integer number of periods by means of the projection of the interferogram of a radial phase-mask [5]. The occurrence of holistic resonant reflection couldn't be established because of the generally admitted great difficulty to diamond-machine a concave cone in a fused silica bloc (a specific collaborative development work is in progress with the Fachbereich SciTech of Ernst-Abbe-Hochschule Jena). Having the grating waveguide at the inner wall of a fused silica tube easily permits the reflective cone to be inserted into the tube hollow to generate the desired incident cylindrical wave, and pick up the expected resonant reflection although the concentricity of the cone and tube wall is difficult to ensure.

2. Structure Design

The determination of the grating waveguide opto-geometrical parameters is first made in a planar geometry. This is reasonable since the ratio between the tube inner radius R ($R \cong 4$ mm) and the wavelength λ (λin the 1300–1600 nm range) is of the order of 10^3. The conditions for resonant reflection to occur in a cylindrical wave excitation similarly to the planar counterpart were investigated theoretically [8] with the conclusion that 100% reflection coefficient is obtained once the curvature radius is larger than about 10 grating periods; this condition is amply satisfied here. The same authors analyzed theoretically the resonance characteristics of a cylindrical grating waveguide excited by a cylindrical wave [9] under the same conditions of very small curvature radius by expressing the field in terms of Bessel functions; the issues of design and fabricability were not addressed.

The most appropriate deposition technology of a uniform waveguide layer at the inner wall of a silica tube would ideally be that of fiber preform CVD chemical vapor deposition; however, we had to resort to a lighter laboratory technique: the coupled waveguide structure is here composed of a non-corrugated uniform TiO_2 sol-gel layer of thickness w_g and refractive index $n_g = 1.7$, and a binary photoresist corrugation of 0.5 duty cycle, depth d and refractive index $n_{gg} = 1.67$. There is air in the fused silica tube of refractive index $n_s = 1.45$. To prevent diffraction orders in the silica tube, and spurious resonant reflections in the considered wavelength range, the grating-waveguide equivalent thickness w_{eq} will be set between the cutoff thickness w_{c0} of the fundamental TE_0 mode at the large wavelength $\lambda_L = 1600$ nm of the wavelength range, and the cutoff thickness w_{c1} of the first higher order TE_1 mode at the small wavelength $\lambda_S = 1300$ nm of said range. The equivalent grating-waveguide thickness w_{eq} is defined as the thickness of a gratingless uniform equivalent waveguide having the permittivity n_g^2 of the actual waveguide for the TE polarization:

$$w_{eq} = w_g + d.\frac{1 + n_{gg}^2}{2n_g^2} \tag{1}$$

Setting the effective index n_e of the TE_0 and TE_1 modes to n_s in the TE dispersion equation defines the TE_0 and TE_1 mode cutoff thicknesses w_{c0} and w_{c1}, and gives the range of w_{eq} for single mode operation:

$$\frac{\lambda_L}{2\pi\sqrt{n_g^2 - n_s^2}} arctan\sqrt{\frac{n_s^2 - 1}{n_g^2 - n_s^2}} < w_{eq} < \frac{\lambda_s}{2\pi\sqrt{n_g^2 - n_s^2}}\left(arctan\sqrt{\frac{n_s^2 - 1}{n_g^2 - n_s^2}} + \pi\right) \tag{2}$$

The above condition (Eq. 2) leads to 250 nm $< w_{eq} <$ 935 nm with the present choice of materials and wavelength range. As will be described in Section 3, the technological constraints imposed by the sol-gel and photoresist coating at the tube inner wall prescribe w_g and d in the range of 700 nm, i.e., w_{eq} about 600 nm according to Eq. 1 which is well in the single mode operation range. Solving the TE dispersion equation for the equivalent waveguide gives a TE_0 mode effective index n_e of 1.55; under normal incidence the grating permitting the coupling of a plane wave to the

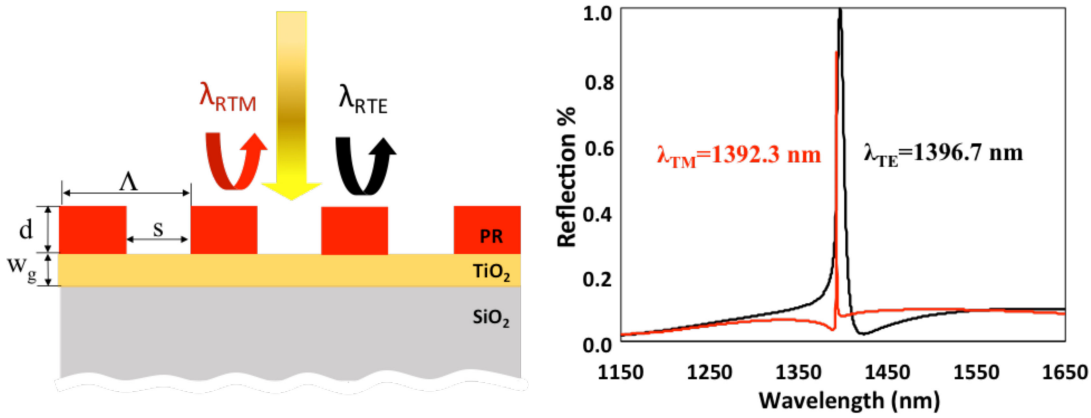

(a) (b)

Fig. 1. Planar waveguide grating modeling of TM and TE polarization resonant reflections (red and black lines, resp.) under normal incidence. $w_g = 205$ nm, $d = 554$ nm, $\Lambda = 960$ nm, $s = 480$ nm. $n_{SiO2} = 1.45$; $n_{TiO2} = 1.7$; $n_{PR} = 1.67$. (a) Cross-section of the diffractive structure, (b) calculated spectra.

TE_0 mode has a period Λ given by $\Lambda = \lambda/n_e$, i.e., Λ between 900 and 1030 nm. The period $\Lambda = 960$ nm is chosen for the planar experimental simulation. The fabricated planar grating waveguide structure illustrated in Fig. 1 has a measured sol-gel layer thickness of 205 nm, a photoresist grating depth of 554 nm (so shallow a waveguide thickness is dictated by the TiO_2 sol-gel layer preparation technology and pulling deposition technique). The TE and TM reflection spectra under normal incidence are calculated rigorously by means of the collinear modal code of MC Grating [10] and illustrated in Fig. 1 assuming the corrugation to have a 0.5 duty cycle and vertical walls. The resonant reflection due to the TE_0 mode coupling takes place at $\lambda_{RTE} = 1396.3$ nm whereas that due to the TM_0 mode coupling occurs at $\lambda_{RTM} = 1392.3$ nm which corresponds to an expected lower, but actually quite close, effective index.

Worth noting at this point is the very large difference between the TE and TM resonance widths. The FWHM of the TE and TM 100% reflection peaks is 8 and 0.7 nm respectively. This has a major consequence on their experimental detectability by means of a spectrometer of finite spectral resolution. This spectral width discrepancy is a result of the large difference between the TE and TM waveguide mode radiation coefficients under normal incidence [7]. A further reason for the narrowness of the TM reflection peak lies in the weak guidance of the rather thin waveguide layer imposed by the sol-gel deposition technique: whereas the TE_0 effective index given by $\lambda_{TE}/\Lambda = 1.455$ is well above the substrate index 1.45, that of the TM_0 mode is 1.4503, very near to its cutoff; this implies that the normalized modal electric field in the grating volume is very weak; so is the radiation coefficient. It is therefore expected that the experimental demonstration of the cylindrical wave resonant reflection is likely to only exhibit a TE resonance peak.

3. Fabrication

3.1 Substrate Pre-Treatment and Layer Deposition

The silica surface first undergoes a three-step cleaning process of successive immersion into three ultrasonic baths of acetone, ethanol and pure water. Then, an oxygen plasma treatment enhances its hydrophilicity and creates extra OH bonds for better surface wettability and TiO_2 adhesion. Although the sol-gel TiO_2 could be used for the coupling grating definition thanks to its negative resist property, it will only be used here for the definition of a uniform waveguide layer.

The preparation of the TiO_2 solution involves a succession of hydrolysis-condensation reactions at the molecular level [11]. The synthesis protocol is fully described in previous articles [12], [13].

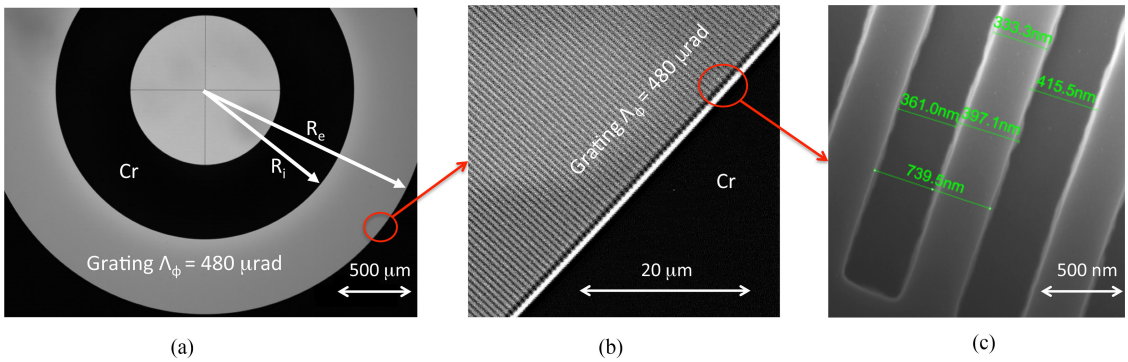

(a) (b) (c)

Fig. 2. Images of the radial phase-mask grating by optical microscopy: (a) of the whole element, (b) zoom at the external border and (c) by SEM at the larger (R_{ext}) radii.

The sol-gel deposition is dip-coated at a 7 cm/min rate. The pulling speed is initially tested on flat fused silica substrates before being applied to the cylindrical tubes; it leads to thick and uniform deposits with reduced evaporation rate. The obtained layer is first dried at room temperature and then post-baked at 110 °C during 3 hours; this leads to a stabilized xerogel layer in amorphous phase of 205 nm thickness as measured by profilometer. It is assumed that the same coating process leads to nearly the same thickness at the outer and inner walls of the tubes because of the large diameter. A layer of positive photoresist (S1805) diluted with 50% ethyl lactate is coated similarly on the xerogel layer and soft baked at 60 °C during 1 min. The obtained resist layer thickness is found to be 555 nm.

3.2 Cylindrical Grating Patterning

The cylindrical grating pattering is interference photolithography under light exposure through a phase-mask of radial geometry to a photosensitive resist layer at the inner wall of the tube. The phase-mask consists of a binary corrugation in a fused quartz substrate defined by e-beam lithography and etched by reactive ion etching. It has been designed to maximize the amplitude of the transmitted 1st order over the full range of period between the inner (480 nm) and outer (720 nm) periods of the radial corrugation under normal exposure at 355 nm wavelength. This leads to a SiO_2 grating depth of 400 nm and 0.54 line/space ratio. The phase-mask angular period is $\Lambda_\phi = 480$ μrad which creates an exposure interferogram of $\Lambda_\phi/2 = 240$ μrad angular period, thus a grating of 26180 lines at the wall of the tube. Assuming the tube inner radius to be $R =$ 4 mm as given in its specifications, the grating period at the inner wall is $\Lambda = R\Lambda_\phi/2 = 960$ nm (Fig. 2). The details on the phase-mask design and fabrication are given in [4].

This phase-mask transfer technology requires a single-step exposure and produces an interferogram of high contrast since the zero order is transmitted parallel to the tube axis, thus does not interfere with the 1st orders at the cylinder wall, and the 2nd diffraction orders are evanescent. The phase-mask exposure set-up is illustrated in Fig. 3. It comprises an optical bench with a small number of optical components. The collimated beam of a linearly polarized CW laser at 355 nm wavelength impinges normally onto the phase-mask plane. A beam-expander enlarges the beam to ensure a substantial overlap of the phase-mask, and a reasonable dose constancy over its area. The tube is placed against the phase mask so that the incident beam axis and the tube axis are parallel, and the phase-mask center is located on the tube axis. This alignment is very critical to ensure a grating period constancy at the tube inner wall. The tube and phase-masks substrate are placed on micro-displacement platforms with the needed degrees of freedom. The alignment under white light illumination is checked by a camera.

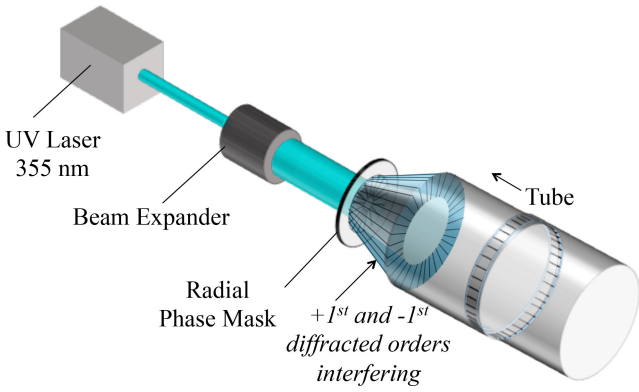

Fig. 3. Cylindrical wall grating exposure set-up.

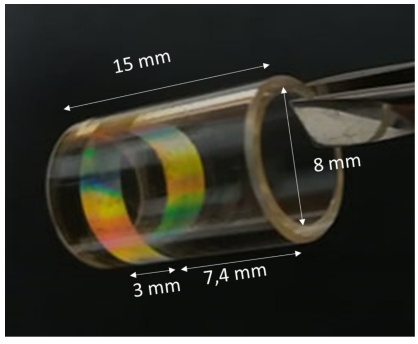

Fig. 4. Final diffraction gratings at the inner wall of a silica tube under white light illumination.

The photosensitive layer at the inner wall of the tube can either be a negative photosensitive sol-gel like TiO_2 which could be used later as an element of a functional device after pyrolysis, or a positive photoresist requiring a further etching process for a physical transfer into the tube wall. At the present stage of development it was preferred to demonstrate the resonant reflection effect with an experimental model whereby the exposed and developed photoresist layer on the uniform TiO_2 layer represent the very grating waveguide in which the resonant effect takes place. The reasons are the much smaller dose needed to expose a photoresist layer (5 second exposure only under 50 mW power), and the complexity of the development process of an exposed sol-gel layer.

Unlike in the case of a grating at the outer wall of a cylinder [4], the structural characterization of a grating at the inner wall of a tube can only be made destructively by growing a metal replica inside the tube. It is however possible to gain some global evaluation of the grating contrast, and especially of its uniformity, by illuminating it under white light as the picture of Fig. 4 illustrates.

4. Resonance Measurement Set-up

The holistic excitation of the grating waveguide at the cylinder inner wall requires a cylindrical wave whose center coincides with the cylinder axis. The needed cylindrical wave is obtained by reflecting a collimated axial beam on a centered metallized cone of 90° apex introduced into the tube hollow. The expected resonant reflection resulting from a waveguide mode excitation is also a cylindrical wave that is reflected by the cone in form of a collimated beam to be analyzed spectrally.

As illustrated in Fig. 5, the spectroscopic bench uses a super continuum source WLSC (200 nm $< \lambda <$ 2400 nm) and a linear IR polarizer LP (650 nm–2 μm) which axis is set at 45° from the axes of a quarter wave-plate. The beam is divided by a 45° beam-splitter BS and impinges onto the

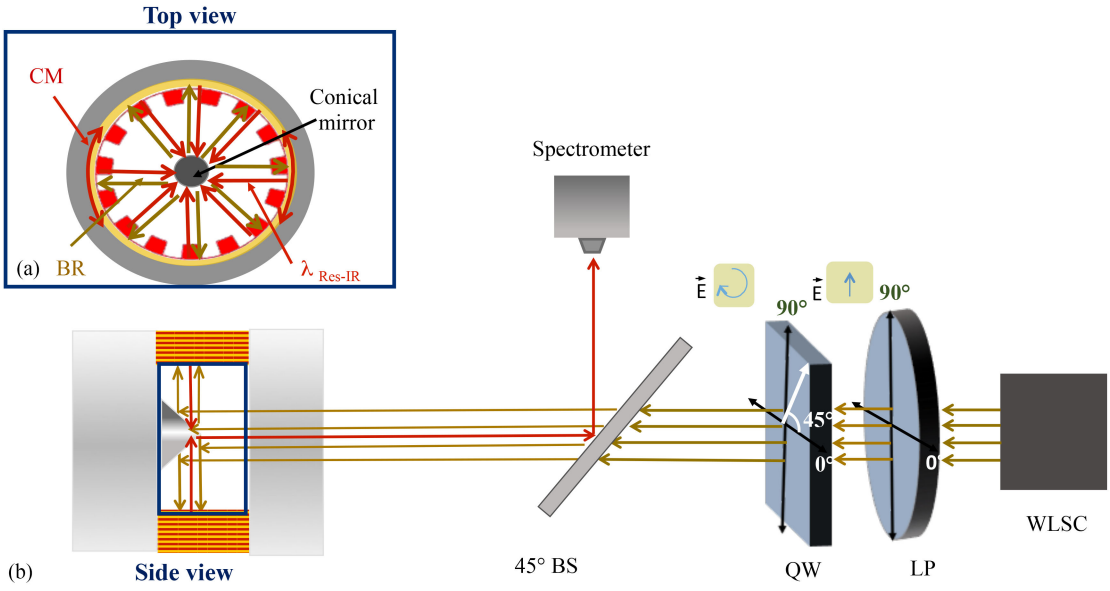

Fig. 5. Spectroscopic set-up for resonance measurement: (a) WLSC white light supercontinuum source, linear polarizer LP, quarter wave plate QW, 45° beam splitter BS, and side view of the metal cone and micro-structured tube, (b) top view of the tube: coupled mode in the waveguide CM, beam reflection BR by the conical mirror and IR resonance.

conical mirror centered on the tube axis where it undergoes a plane to cylindrical wave transform with its k-vector orthogonal to the incident beam axis. The expected resonantly reflected spectral component is directed by the beam splitter to an optical fiber connected to a NIR (900 nm–2100 nm) spectrometer of 24 nm resolution, and is analyzed by a dedicated software.

A polarization-selective measurement of the TE and TM resonant reflections by the cylindrical grating waveguide would imply that the polarization distribution of the incident axial beam is radial and azimuthal respectively. No such wide band polarizing element was available thus a quarter wave element generating a circularly polarized incident coaxial beam was used. Instead of ideally being hit by a normally incident wave of identical linear polarization, each angular element of the cylindrical waveguide grating “sees” the same temporal sequence of incident polarization states; this permits to avoid the effect of the possible and probable layer thickness non-uniformities which a fixed linear polarization of the incident coaxial beam can not average.

The optical measurement set-up was designed to permit the alignment of the cone in the tube center thanks to XYZ and θ_X and θ_Y stages within 5 microns and 0.05 degree accuracy.

5. Results and Discussion

The reference power signal is measured after the beam splitter. The normalized experimental reflection spectrum is plotted in Fig. 6 in arbitrary units together with the simulated TE and TM polarization spectra.

Figure 6 exhibits a definite reflection peak experimentally. The simulated and experimental resonances are spectrally quite close (about 30 nm apart) which indicates that the layer thicknesses obtained at the tube inner wall by dip-coating are close to those obtained with the planar reference sample. The FWHM of the experimental peak is about 40 nm, i.e., five times larger than the calculated TE width, and there is a single peak whereas there should be two under circularly polarized excitation. This is explainable on the basis of the comment made next to Fig. 1 whereby the spectral width of the resonant reflection resulting from a normal TM-polarized excitation is

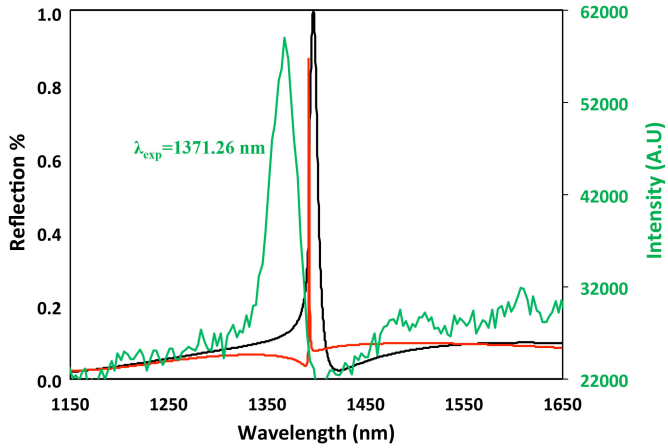

Fig. 6. Superposition of simulated TE and TM spectra (black and red lines, resp.) with the experimental green line in arbitrary units obtained under circular polarization excitation.

much smaller than that of the TE, about 10 times smaller in the present structure. Considering this, furthermore that the TE and TM resonances are theoretically only 4 nm apart, and that the spectrometer resolution is 24 nm, it can be understood that the TE and TM peaks can't be resolved separately; furthermore, their contribution to the total reflected power are in the same ratio as their spectral width, i.e., ten to one. A finer analysis of the resonant reflection characteristics, which is beyond the scope of this paper, would be possible by using a system with very high spectral selectivity at the resonance wavelength [14].

There is something in Fig. 6 much more troublesome however: the ratio λ/Λ of the measured resonance wavelength 1371.26 nm by the assumed period 960 nm gives in principle the effective index n_e of the excited waveguide mode under normal incidence, i.e., $n_e = 1.4284$, which does not correspond to a guided mode since $n_e < n_s = 1.45$, that is, no reflection peak should be observed. The quest for an explanation will first be carried out by a fine characterization of the tube geometry in search for the actual period at the inner wall, then at the more fundamental level of mode coupling under normal incidence.

5.1 Period Determination

The period at the inner wall is determined by the known angular period Λ_ϕ of the phase-mask and by the tube radius *R*. The latter is only approximately known from its specifications; an error on *R* might be the reason for such abnormal effective index value. The sacrificial operation of breaking a tube with its waveguide grating at the inner wall was carried out, permitting the observation of a concave broken piece under SEM. Figure 7 is a top view showing a number of grating periods from where a period of 985.5 nm is retrieved. Using this period instead of 960 nm for the estimate of the effective index aggravates the case: $n_e = 1.391$ is further below the substrate index. An interesting information is gained by observing the cross-section of a broken piece: Fig. 8 reveals that the duty cycle of the photoresist gratings is far from 0.5 and closer to 0.2; the modeling of such structure by using [10] does exhibit a TE_0 reflection peak, but no TM_0 peak which is the conclusive reason for its non-observation.

The fused silica tube has so far been considered as perfectly circular with an inner radius according to the specifications of 4 mm. As the actual period is proportional to the inner radius, a precise determination of the tube geometry was undertaken by Kunz Precision AG by means of a stability and accuracy enhanced EROWA – CMM Qi/CNC measuring machine. The false color results of Fig. 9 on one of the tubes show that the average diameter is 7.8825 mm, the circularity quite good (the diameter varies by $+-3$ nm), and the average diameter varies by $+-10$ nm along

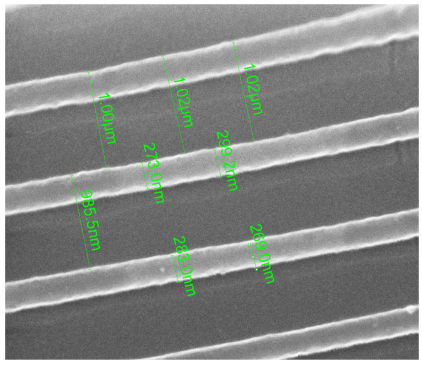

Fig. 7. SEM top view of the photoresist grating.

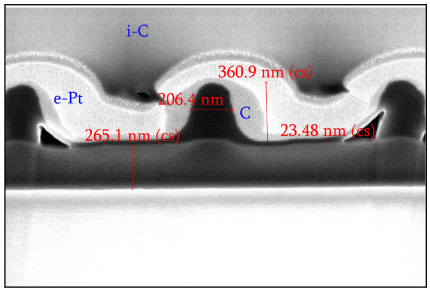

Fig. 8. SEM image of the grating waveguide cross-section.

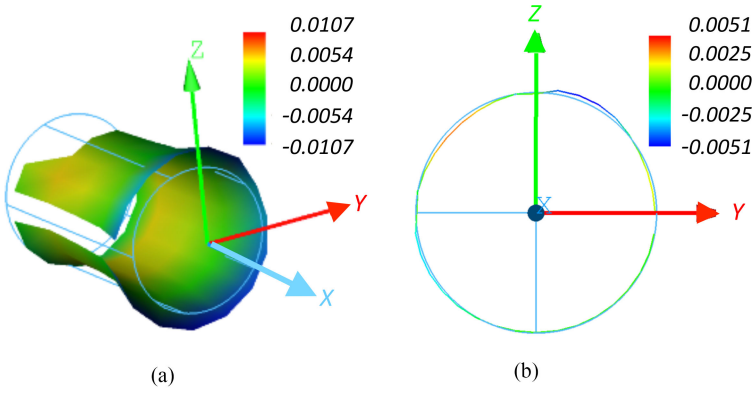

Fig. 9. False color representation of the high precision characterization of the geometry of a tube. (a) diameter variation of $+-10$ nm along the tube axis, (b) inner diameter variations within $+-3$ nm with average diameter 7.883 mm.

the axis. Considering the 240 μrad angular period, the expected period at the inner wall is 946 nm. The measurement of a second tube gives a radius of 3.962 mm, which would lead to a 951 nm period after phase-mask exposure. Comparing the 985.5 nm SEM period of Fig. 7 with the period determined by the precise diameter measurement reveals that the center of the phase-mask was not properly located on the tube axis prior to resist exposure: for the first tube, the measured period of 985.5 nm results from a 4.106 mm distance between the tube inner wall and the phase-mask center instead of about 3.95 mm if the phase-mask was precisely centered on the tube axis. This implies that at the diametrically opposed location on the tube wall the period is 906 nm since the

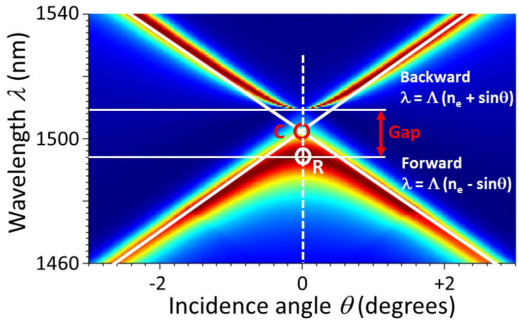

Fig. 10. Dispersion curves of 100% resonant reflection in a $\lambda(\theta)$ diagram close to normal incidence exhibiting the 2nd order gap and vanishing thickness of the large-wavelength branch.

distance between the inner wall and the phase-mask center is there only 3.776 mm. Therefore, the different angular sections of the cylindrical waveguide grating experience slightly different angular and period coupling conditions which inevitably broaden the resulting reflection peak spectrum as observed experimentally (Fig. 6).

Present Section 5.1 elucidates some apparently implausible experimental results from the precise characterization of the cylindrical structure such as resonant reflection from a grating waveguide below the excited mode cutoff wavelength. Such issue must be considered with care from an electromagnetic standpoint also when normal incidence is concerned. This is the subject of next subsection.

5.2 The Inherent Second Order Intra-guide Coupling

Under TE normal incidence the $+$ and -1^{st} order mode coupling is always associated with the 2nd order coupling between the contra-propagating guided modes. This creates a gap in the dispersion curves representing the resonant reflection wavelength versus the incidence angle as shown in Fig. 10 in the neighborhood of normal incidence. The structure considered here is close to that illustrated in Fig. 1 with $w_g = 350$ nm, $d = 600$ nm, and $\Lambda = 1000$ nm; it is calculated by using [10]. In the absence of intraguide coupling the coupling synchronism conditions are represented by the two crossing white lines given by $\lambda = \Lambda\ (n_e + sin\theta)$ for backward coupling by means of the -1^{st} grating order, and $\lambda = \Lambda\ (n_e - sin\theta)$ for forward coupling through the $+1^{st}$ order. The crossing white lines are actually not straight lines since the effective index is a slowly decreasing function of the wavelength.

The crossing point C at normal incidence gives the effective index $n_e = \lambda/\Lambda$ as defined and calculated in Section 2. In the presence of intraguide coupling, however, as it is always the case under normal incidence, the intraguide 2nd order coupling opens a gap whose width is proportional to the 2nd order coupling coefficient where no mode can be excited [15]. Crossing point C is in the gap. The resonance wavelength under normal incidence is given by point R located on the "low-wavelength branch" whose wavelength ordinate is located below that of crossing point C whereas the thickness of the large wavelength branch tends to zero under normal incidence. Considering R's ordinate for estimating the effective index as made after Fig. 1 leads to too small an estimate of n_e.

6. Summary and Conclusion

Despite the technical and characterization difficulties the present paper makes the experimental demonstration that the phenomenon of resonant reflection of a plane wave at a planar waveguide grating also exists in a cylindrical concave geometry where the radius is much larger than the wavelength. A cylindrical diffractive waveguide device is not just a rolled-up planar device: there is

a major spatial coherence problem in that the grating must have an integer number of periods over 2π. Once this is achieved, as it was here, one immediately sees an essential difference between planar and cylindrical geometries: except in cases where there is a very large 2nd order intraguide coupling coefficient, a very narrow resonance in a planar geometry requires an infinitely long and very low efficiency grating addressed by a plane wave of infinite extent, whereas the same spectral width can be achieved with a waveguide at the wall of a centimeter size cylinder coupled by a stitchingless grating addressed by a cylindrical wave, the coupled guided mode having a multi-turn propagation length.

The experimental results obtained here where not intended to lead to applications although the presence of a sensor transducer at the hollow of a tube may be seen as configurationally compatible with a gas flow in the very same tube. The aim was rather to make the experimental demonstration of the very waveguide grating resonant reflection in a cylindrical geometry. This could not be made with a waveguide grating at the surface of a solid cylinder because of the impossibility to have a concave cone machined in fused silica. This manufacturing problem has now been solved and early results will soon be published.

Acknowledgment

The authors are grateful to Kunz Precision AG, 4800 Zofingen, Switzerland, for the high accuracy measurement of the tube inner diameter, and of its circularity.

References

[1] G. A. Golubenko, A. S. Svakhin, V. A. Sychugov, and A. V. Tishchenko, "Total reflection of light from a corrugated surface of a dielectric waveguide," *Sov. J. Quantum Electron.*, vol. 15, no. 7, pp. 886–887, 1985.
[2] S. S. Wang and R. Magnusson, "Theory and applications of guided-mode resonance filters," *Appl. Opt.*, vol. 32, no. 14, pp. 2606–2613, 1993.
[3] Y. Fang, A. M. Ferrie, N. H. Fontaine, J. Mauro, and J. Balakrishnan, "Resonant waveguide grating biosensor for living cell sensing," *Biophys. J.*, vol. 91, no. 5, pp. 1925–1940, 2006.
[4] L. Berthod *et al.*, "Efficient reversible phase mask for TiO_2 submicron gratings directly printed on cylindrical surfaces," *Opt. Express*, vol. 25, no. 8, pp. 9003–9009, 2017.
[5] S. Tonchev *et al.*, "Subwavelength cylindrical grating by holistic phase-mask coordinate transform," *Opt. Express*, vol. 20, no. 7, pp. 7946–7953, 2012.
[6] O. Parriaux, Y. Jourlin, and N. Lyndin, "Cylindrical grating rotation sensor," US Patent US8345259B2, 2013.
[7] I. A. Avrutsky and V. A. Sychugov, "Reflection of a beam of finite size from a corrugated waveguide," *J. Mod. Opt.*, vol. 36, no. 11, pp. 1527–1539, 1989.
[8] Y. Ohtera, S. Iijima, and H. Yamada, "Guided-mode resonance in curved grating structures," *Opt. Lett.*, vol. 36, no. 9, pp. 1689–1691, 2011.
[9] Y. Ohtera, S. Iijima, and H. Yamada, "Cylindrical resonator utilizing a curved resonant grating as a cavity wall," *Micromachines*, vol. 3, no. 1, pp. 101–113, 2012.
[10] MC Grating software, https://mcgrating.com/, 2019.
[11] C. Sanchez, B. Julian, P. Belleville, and M. Popall, "Applications of hybrid organic-inorganic composites," *J. Mater. Chem.*, vol. 15, no. 35–36, pp. 3559–3592, 2005.
[12] O. Shavdina *et al.*, "Large area fabrication of periodic TiO_2 Nanopillars using microsphere photolithography on a photopatternable Sol–Gel film," *Langmuir*, vol. 31, no. 28, pp. 7877–7884, 2015.
[13] S. Briche *et al.*, "New insights in photo-patterned sol–gel-derived TiO_2 films," *J. Mater. Sci.*, vol. 46, no. 5, pp. 1474–1486, 2011.
[14] D. K. Armani, T. J. Kippenberg, S. M. Spillane, & K. J. Vahala, "Ultra-high-Q toroid microcavity on a chip" *Nature*, vol. 421, pp. 925–928, 2003.
[15] F. Pigeon and A. V. Tishchenko, "Modelling of finite-size grating waveguide filters on the basis of a free-space diffraction approach," *Opt. Quant. Electron.*, vol. 34, no. 5/6, pp. 505–521, 2002.